The β-Subunit of the Arabidopsis G Protein Negatively Regulates Auxin-Induced Cell Division and Affects Multiple Developmental Processes[W]

Hemayet Ullah,[a,1] Jin-Gui Chen,[a,1] Brenda Temple,[b] Douglas C. Boyes,[c] José M. Alonso,[d,2] Keith R. Davis,[c] Joseph R. Ecker,[d] and Alan M. Jones[a,3]

[a] Department of Biology, University of North Carolina at Chapel Hill, Chapel Hill, North Carolina 27599-3280
[b] Structural BioInformatics Core Facility, University of North Carolina School of Medicine, Chapel Hill, North Carolina 27599
[c] Department of Plant Research, Paradigm Genetics, Inc., Research Triangle Park, North Carolina 27709-4528
[d] Plant Biology Laboratory, The Salk Institute for Biological Studies, La Jolla, California 92037-1099

Plant cells respond to low concentrations of auxin by cell expansion, and at a slightly higher concentration, these cells divide. Previous work revealed that null mutants of the α-subunit of a putative heterotrimeric G protein (*GPA1*) have reduced cell division. Here, we show that this prototypical G protein complex acts mechanistically by controlling auxin sensitivity toward cell division. Loss-of-function G protein mutants have altered auxin-mediated cell division throughout development, especially during the auxin-induced formation of lateral and adventitious root primordia. Ectopic expression of the wild-type Gα-subunit phenocopies the Gβ mutants (auxin hypersensitivity), probably by sequestering the Gβγ-subunits, whereas overexpression of Gβ reduces auxin sensitivity and a constitutively active (Q222L) mutant Gα behaves like the wild type. These data are consistent with a model in which Gβγ acts as a negative regulator of auxin-induced cell division. Accordingly, basal repression of approximately one-third of the identified auxin-regulated genes (47 of 150 upregulated genes among 8300 quantitated) is lost in the Gβ transcript-null mutant. Included among these are genes that encode proteins proposed to control cell division in root primordia formation as well as several novel genes. These results suggest that although auxin-regulated cell division is not coupled directly by a G protein, the Gβ-subunit attenuates this auxin pathway upstream of the control of mRNA steady state levels.

INTRODUCTION

In the classic paradigm, heterotrimeric GTP binding proteins (G proteins) couple diverse signaling through membrane-delimited, G protein–coupled receptors to downstream effectors, some of which ultimately results in transcriptional control. Binding of a ligand to its cognate G protein–coupled receptors leads to the conversion of an inactive G protein (GDP bound) to its active conformation (GTP bound), which then activates target proteins in the next step of this signal transduction. Known downstream effectors are diverse and include adenylate cyclase, cGMP phosphodiesterase, phospholipase Cβ, phospholipase A2, and potassium channels.

Although the presence of G protein–coupled signal trans-

duction is well documented in metazoa, evidence for a comparable system in plants is scant (reviewed by Assmann, 2002). Genes that encode putative G protein subunits have low sequence identity to known G proteins; thus, the existence of a prototypical G protein in plants remains unproven. However, evidence based on pharmacological experiments suggests a role for a heterotrimeric G protein in various signal transductions, such as for auxin (Zaina et al., 1990, 1991, 1994), abscisic acid (Fairley-Grenot and Assmann, 1991), gibberellin (Jones et al., 1998; Ueguchi-Tanaka et al., 2000), pathogens (Beffa et al., 1995), blue light (Warpeha et al., 1991), and red light (Neuhaus et al., 1993). Recently, genetic evidence has indicated that abscisic acid (Wang et al., 2001) and brassinosteroids (Ullah et al., 2002) use a heterotrimeric G protein in signal transduction.

To date, 23 Gα, 6 Gβ, and 12 Gγ genes have been found in mammals (Vanderbeld and Kelly, 2000). The α-subunits are classified into four subfamilies: G_s, G_i, G_q, and G_{12}. By contrast, based on the essentially complete genome of Arabidopsis, plants have a single candidate gene, *GPA1*, that encodes a prototypical Gα-subunit. GPA1 shares ∼30%

amino acid sequence identity with mammalian Gα-subunits, with slightly higher identity to G_i. Among the G_i subfamily, GPA1 is most similar to G_z, the most divergent member of this group (Jones, 2002). Similarly, based on sequence information alone, there is a single candidate Gβ gene and possibly two Gγ-subunit genes. Unfortunately, structural information, either predicted or empirically derived, for the authentication of an Arabidopsis G protein complex has not been reported; thus, the authenticity of a plant G protein complex has not been proven. However, GTPγS binding to GPA1 (Wise et al., 1997) and a slow GTPase activity for an ortholog of GPA1 (Aharon et al., 1998) have been reported.

The possibility of a single heterotrimeric G protein complex suggests that G-coupled signaling in plant cells must be dramatically less complex than that in animals, but this simplicity raises the question of how such a wide diversity of plant signals can be coupled by a single heterotrimeric complex and how this specificity in transduction is achieved. In assessing this paradox, several questions must be answered. What evidence supports a genuine heterotrimeric G protein complex composed of GPA1, AGB1, and AGG1? What are the signal pathways in which the G protein operates? And what are the relative contributions of the Gα- and Gβ-subunits in these pathways?

Our previous work with Gα protein-null mutants suggested a role for a candidate G protein subunit in cell proliferation and for G protein coupling of auxin-regulated cell proliferation (Ullah et al., 2001). Biochemical evidence for the G protein coupling of auxin signaling has been reported by Zaina et al. (1990). Using a nonhydrolyzable ^{35}S-labeled GTP analog, GTPγS, they found that indole-3-acetic acid (IAA) increased the binding of ^{35}S-GTPγS to rice coleoptile membrane vesicles by twofold compared with the auxin control. This finding indicates that auxin stimulates the exchange of GDP bound on a G protein for a GTP, which is diagnostic of G protein coupling in an auxin pathway.

Auxin regulates lateral and adventitious root formation (Blakely et al., 1988; Laskowski et al., 1995) by controlling the rate of cell elongation in emerging roots and the amount and position of cell division in root primordia formation. Lateral root formation is initiated when a small number of quiescent cells in the root pericycle dedifferentiate and undergo cell division to form the root primordium. Subsequent changes in the positions of division planes and expansion of cells in the primordium have been staged (Malamy and Benfey, 1997), and the cell elongation and cell division processes can be separated genetically (Celenza et al., 1995). Exogenous application of IAA induces lateral root formation (Blakely et al., 1988), and mutants and transgenic plants with increased auxin levels have excess roots compared with the wild type (Klee, 1987; Boerjan et al., 1995). By contrast, application of the auxin transport inhibitor naphthylphthalamic acid (NPA) decreases lateral root formation in tomato (Muday and Haworth, 1994), and the auxin-resistant mutants *axr1*, *axr4*, and *aux1* have significantly fewer lateral roots (Hobbie and Estelle, 1995; Timpte et al., 1995).

gpa1 and *agb1* mutants have altered auxin-induced root formation among other relevant phenotypes. The root phenotype was used here to dissect the specific role of a heterotrimeric G protein in plant cell proliferation and to determine mechanistically which G protein subunit predominates in the auxin signaling pathway in root pericycle cells.

RESULTS

Molecular Modeling Supports GPA1, AGB1, and AGG1 as a Genuine Heterotrimeric G Protein Complex

Experimentally determined structures for two different mammalian G protein heterotrimers have been reported previously. The Protein Data Bank (PDB) model with accession code 1GOT is a 2.0-Å structure of the heterotrimer Gt-α (bovine)/Gi-α (rat) chimera, Gi-β1 (human), and Gt-γ1 (bovine) (Lambright et al., 1996). The model with PDB accession code 1GP2 is a 2.3-Å structure of Gi-α1 (rat), Gi-β1 (human), and Gi-γ2 (C68S) (bovine) (Wall et al., 1995, 1998). The structures of 1GOT and 1GP2 are very similar and superimpose with a root-mean-square deviation of 1.2 Å. The mammalian heterotrimer 1GOT is shown in Figure 1A with the α-, β-, and γ-subunits colored blue, purple, and gold, respectively. The Gα-subunit is composed of an N-terminal helix that interacts with Gβ, a mixed α-helical/β-strand Ras-like domain with GTPase function, and an all α-helical domain. The Gβ-subunit is a seven-bladed β-propeller structure with an N-terminal helix. The γ-subunit contains two helices that interact with the N-terminal helix of the subunit and the β-propeller structure itself.

The higher resolution structure 1GOT was used as a template to build a homology model (Figure 1B; see also supplemental data online) of the Arabidopsis G protein heterotrimer Gαβγ. Models for each of the three subunits were built independently and then superimposed onto the heterotrimer structure of the G protein. The fold-recognition servers BIOINBGU (Fischer, 2000), 3D-PSSM (Kelley et al., 2000), GenTHREADER (Jones, 1999), and FUGUE (Shi et al., 2001) all identified the Arabidopsis sequence GPA1 as a Gα protein with >99% confidence, and all but 3D-PSSM identified the Arabidopsis sequence AGB1 as a Gβ protein with >99% confidence. The 3D-PSSM server selected the seven-bladed β-propeller structure as the most compatible structure with the *AGB1* sequence with 80 to 90% confidence. All of the servers determined the Gγ protein to be the most compatible structure with the Arabidopsis AGG1 sequence, although none of the predictions had >99% confidence. The final theoretical model for Arabidopsis Gα was given a self-compatibility score of 146.9 by the Profiles-3D/Verify module of Insight II. The typical score expected for an experimentally determined protein structure of 362 residues was 165.0, whereas a score of <74.2 was considered indicative of an incorrect structure. For comparison, the self-

compatibility score for the 338-residue mammalian Gα structural template was 148.9, with a typical score of 154.0 and a minimum score of 69.3. Self-compatibility scores of 167.5 and 165.9 were calculated for the theoretical Arabidopsis Gβ structure and the experimentally determined mammalian Gβ, respectively. The Arabidopsis Gβ model contained 362 residues and the typical self-compatibility score was reported at 165.0, whereas the mammalian Gβ contained 339 residues and had a typical self-compatibility score of 154.4. The 786-residue theoretical Arabidopsis heterotrimer had self-compatibility and typical scores of 336.8 and 360.4, respectively. The self-compatibility score for the mammalian composite heterotrimer was 346.9, with a typical score of 331.3 for a 723-residue protein.

The theoretical models (Figure 1B) of the Arabidopsis G protein heterotrimer monomers based on the mammalian templates (Figure 1A) are "valid" structures overall (model deposited at PDB). The compatibility of the Arabidopsis sequences with the mammalian G protein structures was predicted by the fold-recognition servers BIOINBGU, 3D-PSSM, GenTHREADER, and FUGUE. The Profiles-3D/Verify self-compatibility scores indicated that the final theoretical structures for Arabidopsis Gα and Gβ are nearly as compatible with the Arabidopsis sequences as the experimentally determined mammalian structures of Gα and Gβ are with the mammalian sequences. Although the overall structures are valid, there are some minor differences between the Arabidopsis structures and the mammalian structures caused by insertions in the Arabidopsis proteins. The insertions generally are small, with an average size of 5.0 residues for 5 inserts in the Arabidopsis Gα-subunit and an average size of 2.3 residues for 10 inserts in the Arabidopsis Gβ-subunit. The unpredicted conformations are colored green in Figure 1B.

The functionally important regions of the G protein heterotrimer structure are highly conserved in the Arabidopsis heterotrimer. Guanine nucleotide binding proteins contain five conserved sequence elements that are highlighted in Figure 1C. These elements are: (1) the NKxD motif (orange), which interacts with the nucleotide base and is responsible for guanine specificity; (2) the P-loop (green), a GxxxxGKS motif that interacts with the β- and γ-phosphates; (3) the DxxG motif (yellow), which is responsible for distinguishing between GTP and GDP; and the two switches: (4) switch I (red) and (5) switch II (dark blue). Figure 1D, which shows the Arabidopsis heterotrimer in the same orientation as the mammalian heterotrimer in Figure 1C, shows residues highlighted according to the degree of conservation among G proteins. Invariant or highly conserved residues are dark blue, dark magenta, or dark gold in Gα, Gβ, or Gγ, respectively. Conserved residues are correspondingly light blue, light magenta, or light gold. Residues that are not conserved are white in the Arabidopsis heterotrimer. This color scheme is reproduced in Figures 1E and 1F, in which the heterotrimer has been rotated to show the Gα–Gβ interactions (Figure 1E) and the Gβ–Gγ interactions (Figure 1F). The side

chains of residues involved in protein–protein interactions are highlighted and also are colored according to conservation. Residues in Gα that interact with Gβ (Figure 1E) are Ala-7, Ile-10, Glu-11, Ile-14, and Glu-17. Residues in Gβ that interact with Gγ (Figure 1F) are Val-11, Leu-14, Glu-17, Val-27, Ser-28, Leu-34, Leu-48, Leu-49, and Trp-60 (Arabidopsis numbering). Clearly, the sequence elements of the guanine nucleotide binding proteins that are responsible for their action as molecular switches are conserved in the Arabidopsis Gα-subunit. The interface residues involved in formation of the heterotrimer also are highly conserved. A cycling view of the conserved interactions between Gα- and Gβ-subunits and Gβ- and Gγ-subunits, as shown in Figures 1E and 1F, is provided as a video of 5-Å increment rotation in the supplemental data online.

A Transcript-Null Allele of *agb1* and Genetic Complementation

Deconvoluted pools of DNA from T-DNA–transformed plants were screened for insertion in the Arabidopsis *AGB1* gene. A total of 40,000 T-DNA insertion lines in the Columbia ecotype (J.M. Alonso and J.R. Ecker, unpublished data) were screened by PCR using gene- and T-DNA–specific primers (see Methods). A single putative insertion line was identified, and the sequence of the corresponding mutant DNA revealed that the T-DNA insertion was in the fourth exon of the *AGB1* coding sequence (Figure 2A). Segregation of the kanamycin-resistant marker among an F2 population indicated a single T-DNA insertion event (data not shown). Reverse transcriptase–mediated PCR of cDNA isolated from homozygous mutant plants failed to detect an *AGB1* transcript, indicating that individuals homozygous at the mutant *AGB1* locus are transcript null (Figure 2B). The mutant described here is designated *agb1-2* because after completion of the T-DNA screen, another mutant allele of *agb1* was reported from a genetic screen for additional loci in the ERECTA receptor kinase signaling pathway (Lease et al., 2001). This putative protein-null mutant, *agb1-1*, contains a missense mutation in an intron splice site, resulting in the addition of 20 novel amino acids to a truncated AGB1.

Insertion of a T-DNA in the fourth exon of the *agb1-2* coding sequence would effectively render the protein nonfunctional as a result of a change in the coding register of the conceptually translated mRNA and the introduction of a premature stop codon, thus eliminating the seven-bladed propeller structure and the predicted contact residues with the Gγ-subunit. It has been shown that a truncation mutant consisting of the first 41 amino acids of AGB1 cannot interact with the putative Arabidopsis Gγ-subunit (Mason and Botella, 2000). Moreover, the loss of blade 7, as predicted for AGB1, has been shown to disrupt the association with Gα (Clapham and Neer, 1997).

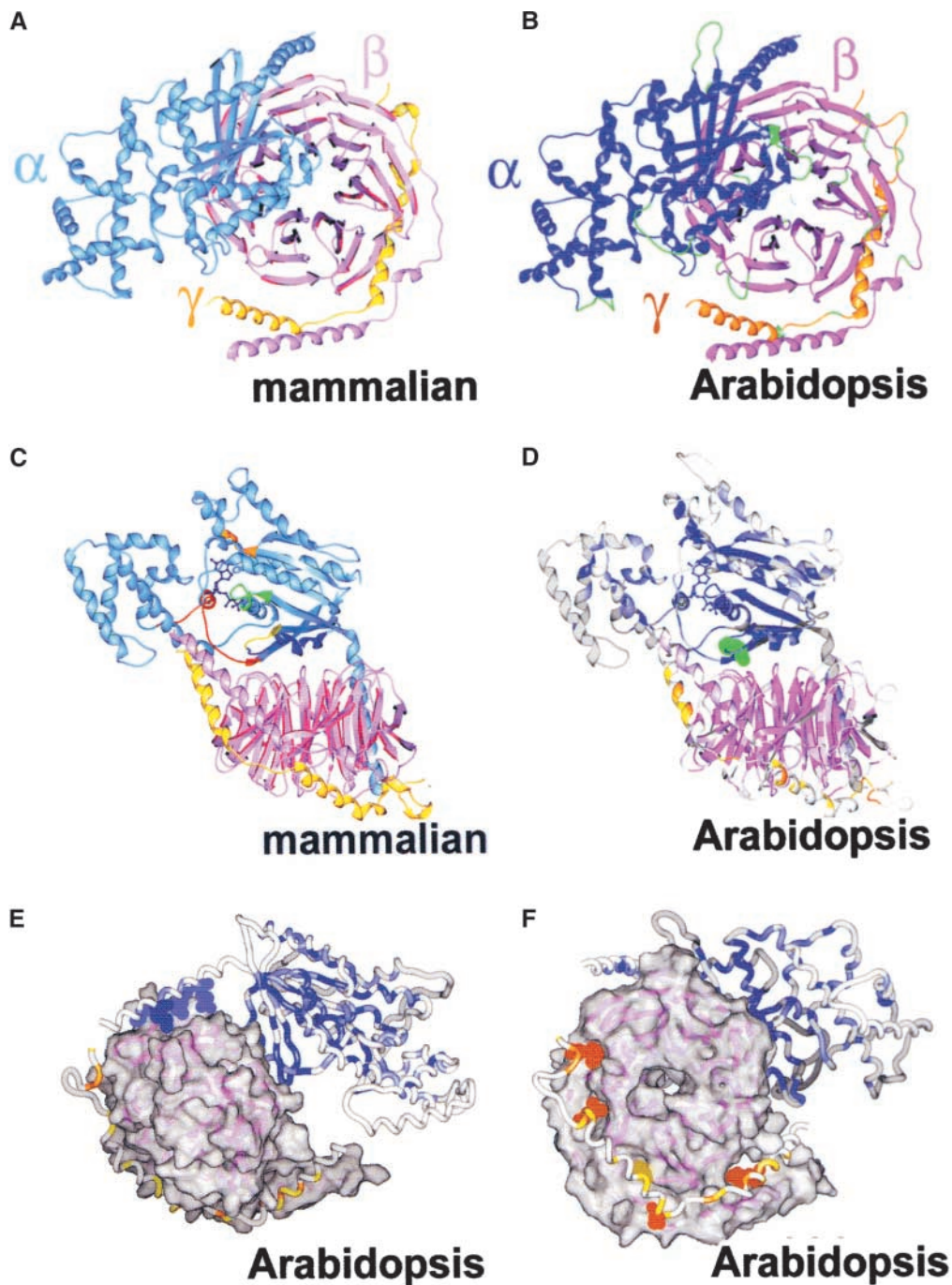To confirm that the *agb1-2* phenotype is caused by the T-DNA insertion, genetic complementation was performed

Figure 1. Modeling the Arabidopsis Heterotrimeric G Protein Complex.

(A) and **(B)** Homology models were built for the GPA1, AGB1, and AGG1 deduced protein sequences from Arabidopsis using the Insight II molecular modeling system from Accelrys, Inc. The macromolecular structures were built using an experimentally determined structure of a mammalian G protein heterotrimer (PDB access code 1GOT.pdb) as the template. The structure of the mammalian heterotrimer used as the template is shown in **(A)**, and the predicted structure of the Arabidopsis G protein heterotrimer is shown in **(B)**. The α-monomers are shown in cyan, the β-monomers are shown in magenta, and the γ-monomers are shown in gold.

(C) The conserved elements of the guanine nucleotide binding domain in the mammalian Gα protein. The P-loop, switch I, and switch II elements are indicated in green, red, and dark blue, respectively. Two conserved sequence elements are the DxxG and NKxD motifs; these are indicated in yellow and orange, respectively.

by transforming the *agb1-2* plants with a dexamethasone-inducible *AGB1* cDNA. The construct rescued Agb1⁻ phenotypes in a dexamethasone-inducible manner (complementation shown in Figure 6). Genetic complementation of *agb1-2* is discussed after a full description of the Agb1⁻ phenotypes described in Figures 3 to 6.

Etiolated and Light-Grown Phenotypes of *gpa1* and *agb1* Mutants

The partial de-etiolated phenotype of *agb1-2* (Figures 2C and 3A), which is similar to the reduced cell division observed in the *gpa1* mutants (Ullah et al., 2001), prompted a parallel examination of the cell number and length of *agb1* mutants. Like *gpa1*, the *agb1* mutants may have a reduced number of epidermal cells in the hypocotyls that expand to wild-type lengths (Figure 3B). In contrast to *gpa1*, *agb1* hypocotyls are wider than wild-type hypocotyls. A cross-sectional view of the hypocotyl reveals that the increased girth of the hypocotyl is attributable to an increase in both the diameter of cortical cells and the number of epidermal cells (Figure 3C). Thus, although axial cell division is reduced, circumferential division is increased. Otherwise, both mutants contain the wild-type number of cell layers and wild-type histology. *agb1* and *gpa1* leaves both have rounded lamina compared with their respective ecotypes, but *agb1* lamina differ from *gpa1* lamina as a result of the presence of islands of small cells that create a crinkly surface (Figure 3D).

Opposite phenotypes of *gpa1* and *agb1* mutants are apparent in mature plants. Although *agb1* plants display increased apical dominance relative to the wild type (Figure 3E), *gpa1* plants have decreased apical dominance (Figure 3F). Interestingly, *agb1* mutants have increased root mass compared with the wild type, and the opposite occurs with *gpa1* mutants (cf. Figures 3G and 3H). The fruit phenotype of *agb1-2* confirms the observation reported by Lease et al. (2001) that *agb1* siliques are shorter and wider than wild-type siliques (Figure 3J). *gpa1* siliques do not share this Agb1⁻ silique phenotype (Figure 3I). Constitutive overexpression of *GPA1* (line D5) causes a shorter silique size similar to that in *agb1* mutants, although to a much greater degree (Figure 3I). The cellular basis for these altered fruit phenotypes remains unknown.

Phenomics Profiling of *gpa1* and *agb1* Mutants throughout Development

The mutants, grown side by side with their corresponding wild-type ecotypes, were subjected to an exhaustive profiling of their phenotypes from seedling to senescence using the Paradigm Genetics, Inc., phenotypic analysis platform (Boyes et al., 2001). A set of 40 quantitative measurements were made at defined growth stages during Arabidopsis development, and mean values of these traits in the mutants were tested for significant deviation from the corresponding values in the wild type by pair-wise, two-sample Student's *t* tests. Mean values were derived from the analysis of 14 replicate plants per trait on average (see supplemental data online). The *t* test results indicate the normalized difference between the mean response for the mutant and the mean response for the wild type and can be represented in units of standard error (Figure 4). A value of zero indicates concordance with the wild-type trait value, whereas positive and negative *t* values indicate the relative degree to which the mutant trait value is larger or smaller, respectively. In this data set, *t* values of >2 standard errors from the wild-type mean are expected to occur by chance <5% of the time ($P < 0.05$).

The diagonal outcome of the comparison between the two protein-null *gpa1* alleles (Figure 4A) indicates that these two allelic mutants share phenotypes both qualitatively and quantitatively, whereas the two Gβ mutants clearly differ in their quantitative deviation from the wild-type trait value (Figure 4B). The lack of perfect correlation between the *t* test values of the two *agb1* alleles indicates that they do not share a complete set of phenotypes. *agb1-1* was proposed to be a protein-null mutant, but this was not tested directly (Lease et al., 2001). Another possible reason for differences between the two *agb1* alleles is the presence of second-site mutations. Because *agb1-2* is a confirmed transcript-null mutant caused by a single T-DNA insertion (Figure 2B), only this mutant was used for a direct comparison with *gpa1*.

Figure 1. (continued).

(D) The heterotrimer from Arabidopsis in the same orientation as the mammalian heterotrimer shown in **(C)**. These residues, however, are colored according to sequence conservation. Residues in GPA1 that are highly conserved within the 119 Gα sequences found in the ExPaSy SWISS-PROT database (www.expasy.ch) are colored dark blue, and residues that are moderately conserved are colored medium blue. Similarly, residues in AGB1 that are highly conserved among the 30 Gβ proteins found in this database are colored dark magenta, and residues that are moderately conserved are colored lighter magenta. Residues highly conserved among the 27 Gγ sequences are colored dark gold, and residues moderately conserved are colored lighter gold. Regions of the heterotrimer that are not conserved among the G proteins are colored white.
(E) and **(F)** Residues that are important for the α–β interaction in the mammalian structure are highlighted in the Arabidopsis structure shown in **(E)**. The heterotrimer scheme is based on conservation as described for **(D)**. The residues highlighted in **(F)** are the residues important for the β–γ interaction. Note that the residues in both α and γ that interact with β are conserved among all of the G proteins. Rotating views of the structures in **(E)** and **(F)** are available in the supplemental data online.

The pair-wise comparison of t values between the wild-type means for the *gpa1-2* and *agb1-2* mutants reveals several interesting points (Figure 4C). First, many altered phenotypes are shared by both mutants, as indicated by those values that fall along the diagonal two t test values away from zero. For example, fruit and seed weights are greater for both mutants compared with the wild type, and several seed and leaf shape properties are shared by both G protein mutants. Second, several phenotypes are unique to one mutant. *gpa1* pedicels are uniquely long, whereas root properties are altered in the *agb1* mutants. *agb1* flowers and fruits are uniquely different from those of the wild type. Third, some traits are opposite in the two G protein subunit mutants. For example, *gpa1* sepals are longer, whereas *agb1* sepals are shorter, than wild-type sepals. *agb1* seedlings are larger, whereas *gpa1* seedlings are smaller, than wild-type seedlings.

This comparison of the global phenotypic profiles of the two G protein mutants suggests that some development is mediated predominantly by Gα and some is mediated predominantly by Gβγ. Because acquisition of the Gα active conformation requires functional Gβγ subunits to associate the complex with the receptor, phenotypes shared by both mutants indicate developmental pathways in which Gα acts independently of or in positive coordination with Gβγ. On the other hand, because Gβγ is capable of interacting with its effector simply by release from the heterotrimeric complex, phenotypes unique to the Gβ mutant or opposite to the Gα mutant phenotype suggest that the predominant subunit in that developmental pathway is Gβ.

Auxin-Regulated Cell Expansion May Be Normal in *gpa1* and *agb1* Mutants

Many of the G protein mutant phenotypes shown in Figures 3 and 4 suggest that the defect resides in either auxin-induced cell division or elongation pathways. Two assays were performed to examine the inhibitory and stimulatory effects of auxin on cell expansion. Five-day-old *gpa1* and *agb1* mu-
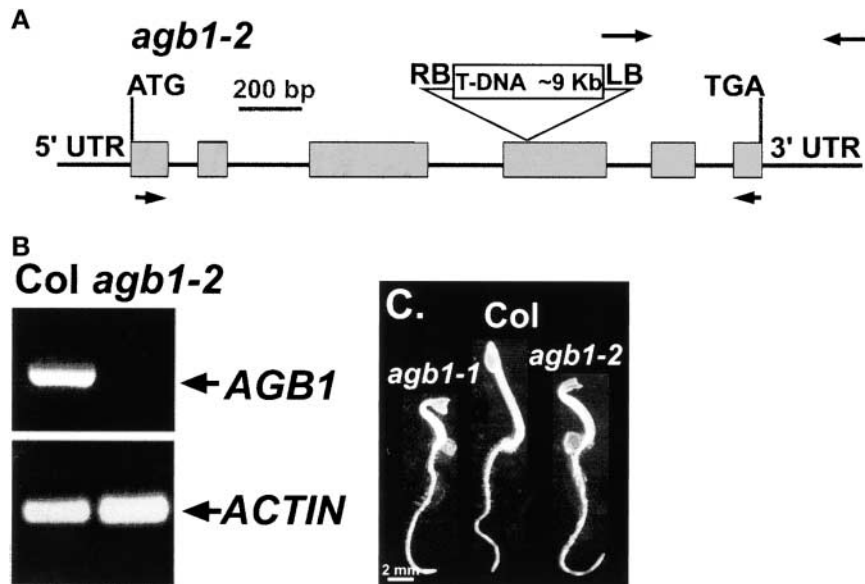

Figure 2. Isolation and Genetic Characterization of the *agb1-2* Mutant.

(A) T-DNA insertion site in AGB1. Gray boxes represent exons. The T-DNA insert is not drawn to scale. The large arrow at the left border indicates the T-DNA left border primer, and the large arrow at the 3′ untranslated region indicates the *AGB1*-specific reverse primer located 200 bp 3′ to the stop codon. LB, T-DNA left border; RB, T-DNA right border; UTR, untranslated region.

(B) Reverse transcriptase–mediated PCR analysis of the *AGB1* transcript. *AGB1* transcript was present in the wild-type (Columbia [Col]) lane (left), but the transcript was absent in the *agb1-2* knockout allele (right lane). Total RNA (2.5 μg) from 5-day-old, dark-grown seedlings was used for cDNA synthesis as a template for the PCR. A forward primer (small arrow at the 5′ end in **[A]**) that spans the transcript initiation site of *AGB1* and a reverse primer (small arrow at the 3′ end in **[A]**) that spans the stop codon were used to perform PCR. As a control, actin primers that amplify a 901-bp product were used to perform PCR on the same cDNA templates. The presence of actin transcript in both lanes indicates that the integrity of RNA quality was not compromised.

(C) Phenotype of 2-day-old, dark-grown seedlings. Wild-type (Columbia [Col]) and mutant seedlings were grown in the dark for 2 days on 1 × Murashige and Skoog (1962) salts, pH 5.7, 0.8% agar, and 1% Suc. The *agb1-1* allele is an independently isolated ethyl methanesulfonate mutant (Lease et al., 2001). Bar = 2 mm.
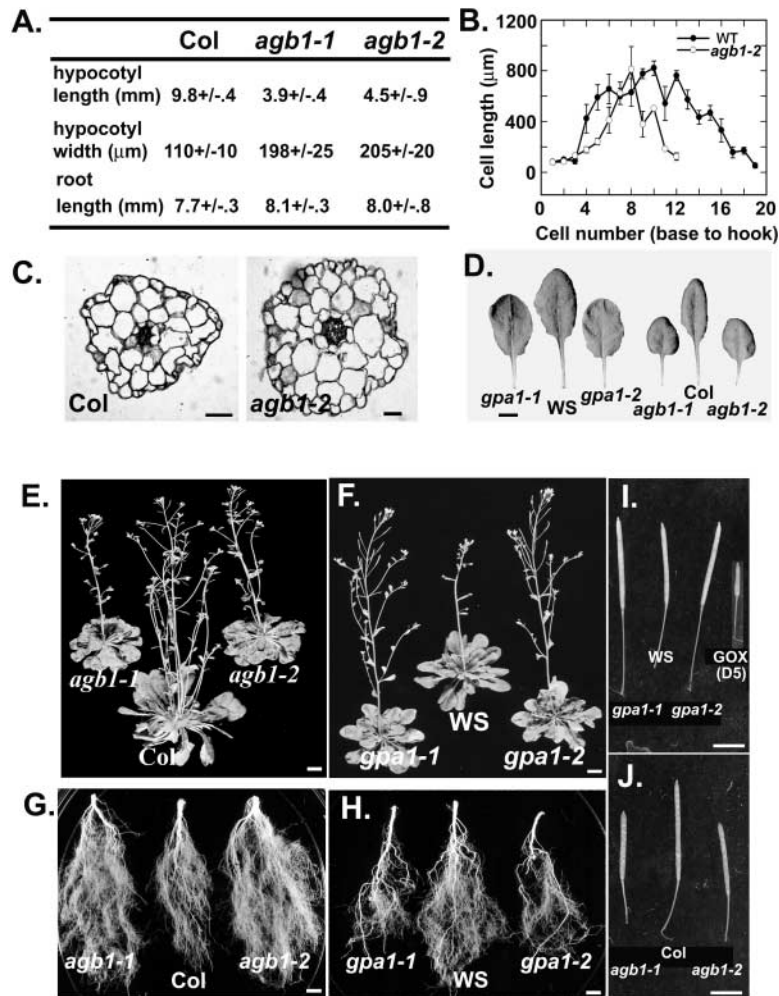
Figure 3. G Protein Mutant Phenotypes.

(A) Effect of a knockout mutation in *AGB1* on hypocotyl length, width, and root length. Standard error of the mean is based on a minimum of 10 seedlings.

(B) Cell sizes along the hypocotyl of *agb1-2*. Cell sizes from the base to the top of the hypocotyls are shown. WT, wild type.

(C) Cross-sections of 2-day-old, dark-grown seedlings. Bars = 15 μm.

(D) Leaf phenotype of 3-week-old, light-grown plants. The genotypes are indicated at bottom. WS, Wassilewskija. Bar = 5 mm.

(E) and **(F)** Mature plant phenotypes. The indicated genotypes were grown in short days (8-h-light/16-h-dark regimen) for 3 weeks and then transferred to long days (16-h-light/8-h-dark regimen) for 2 weeks. Bars = 15 mm.

(G) and **(H)** Mature root phenotypes. Plants were grown in identical conditions as in **(E)** and **(F)**. Bars = 5 mm.

(I) and **(J)** Mature silique morphology. The mutant genotypes are described in Figure 2, in Ullah et al. (2001), and in Lease et al. (2001). Line D5 constitutively expresses *GPA1* (GOX). Bars = 5 mm.

tants along with their respective wild-type ecotypes were transferred to plates supplemented with different concentrations of auxin. The lengths of the roots and hypocotyls were measured 4 days later. The inhibition of root elongation (see supplemental data online) and hypocotyl elongation (data not shown) in the G protein mutants was statistically the same as that in the wild type.

The second assay for auxin-induced cell expansion also indicated wild-type sensitivity to auxin for the G protein mutants. This assay, developed by Gray et al. (1998), took advantage of the temperature dependence of the endogenous auxin pool size. At an increased temperature, free auxin is increased in hypocotyls and manifests as increased growth. The growth of the hypocotyl was shown to be attributable entirely to increased cell elongation. Hypocotyl lengths in G protein mutants at low and increased temperatures were
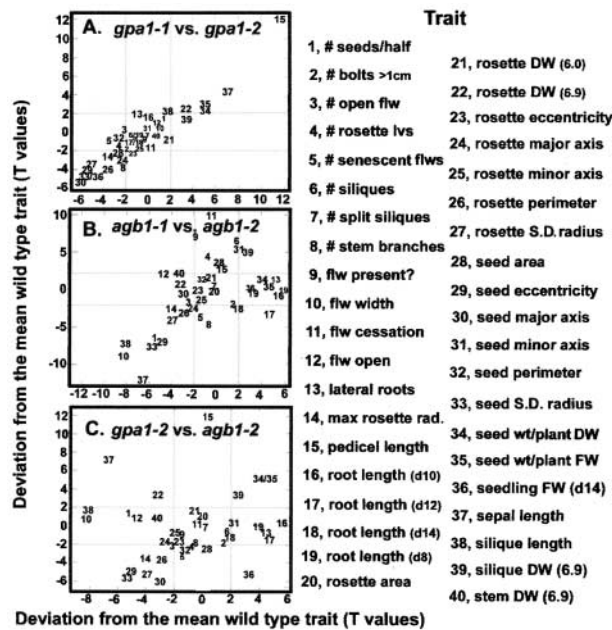
Figure 4. Quantitative Analysis of *gpa1* and *agb1* Developmental Phenotypes from Plants Grown under Standardized Nonstressed Conditions.

Data representing 40 traits from the mutant lines are presented in units of standard error from the wild-type mean. Values >2 or <−2 are considered significant (P < 0.05), and the corresponding thresholds are indicated with gray lines.
(A) Scatterplot of data from *gpa1-1* versus *gpa1-2*.
(B) Scatterplot of data from *agb1-1* versus *agb1-2*.
(C) Scatterplot of data from *gpa1-2* versus *agb1-2*.
Trait descriptions (see Boyes et al., 2001, for details) are as follows: # seeds/half, number of fully developed seeds on one side of a mature silique; # bolts >1cm, number of inflorescence bolts > 1 cm in length per plant at the completion of flowering (growth stage 6.9); # open flw, number of open flowers per plant when >50% of the experimental population had completed flowering (growth stage 6.9); # rosette lvs, number of rosette leaves produced before the transition to flowering (growth stage 5.10); # senescent flws, number of senescent flowers per plant when >50% of the experimental population had completed flowering (growth stage 6.9); # siliques, number of siliques produced per plant; # split siliques, number of split siliques per plant at the completion of flowering (growth stage 6.9); # stem branches, number of lateral branches emanating from the primary inflorescence at the completion of flowering (growth stage 6.9); flw present?, days to first bud observed (growth stage 5.1); flw width, maximum width across the face of the open flower (average of three flowers per plant); flw cessation, days to the cessation of flowering (growth stage 6.9); flw open, days to first flower opening (growth stage 6.0); lateral roots, number of lateral roots per seedling; max rosette rad., maximum rosette radius achieved during the life of the plant; pedicel length; length of pedicel of the mature second flower (growth stage 6.5); root length, length of the primary root (growth day is given in parentheses); rosette area, exposed leaf area of rosette when the first flower is open (growth stage 6.0); rosette DW, dry weight of rosette (growth stage given in parentheses); rosette eccentricity, rosette shape quantitation (growth stage 6.0); rosette

statistically the same as those in the wild type based on pair-wise Student's *t* tests (see supplemental data online).

agb1 Mutants Have Excessive Lateral Root Primordia That Develop More Rapidly

We focused on the root phenotype because it offers a model system for the coordination of auxin-induced cell division with auxin-induced cell expansion. Protrusion of the lateral roots occurs primarily by cell elongation, whereas the number of lateral roots is established by cell division (Malamy and Benfey, 1997). Therefore, the higher number of lateral roots observed for the *agb1* mutants could result from the increased rate of cell elongation from a wild-type number of primordia or from excessive primordia formation. Lateral root primordia of wild-type and mutant roots were scored along the root, and the number, position, and developmental stage of primordia are displayed in spiderweb graphs (Figure 5). The density of threads visually depicts the relative primordia density. Note that *agb1* roots have an approximately twofold greater primordia density than wild-type roots, whereas *gpa1* roots have twofold less primordia density. Twin primordia were observed frequently in *agb1* roots but never in wild-type and *gpa1* mutant roots. Although the greater density of lateral roots in *agb1* mutants suggested excessive cell division, the developmental stage of lateral roots in *agb1* at any comparable position is advanced compared with that in the wild type, indicating that *agb1* root cells may elongate slightly faster as well. The difficulty in visually scoring primordia in stages I and II was addressed by the experimental modification described below.

Auxin-Induced Cell Division Is Negatively Regulated by AGB1

The opposite root phenotypes of *agb1* and *gpa1* suggest that Gβγ, rather than Gα, is the predominant signaling fac-

major and minor axes, rosette size quantitation (growth stage 6.0); rosette perimeter, perimeter of intact rosette (growth stage 6.0); rosette S.D. radius, rosette shape quantitation (growth stage 6.0); seed area, area of individual seeds; seed eccentricity, shape quantitation of individual seeds; seed major and minor axes, size quantitation of individual seeds; seed perimeter, perimeter of individual seeds; seed S.D. radius, shape quantitation of individual seeds; seed wt./plant DW, dry weight of seed produced per plant; seed wt./plant FW, fresh weight of seed produced per plant; seedling FW, fresh weight of the entire seedling at day 14; sepal length, sepal length (average of three flowers per plant); silique length, silique length (average of three siliques per plant); silique DW, dry weight of siliques per plant (growth stage 6.9); stem DW, dry weight of inflorescence stem tissue per plant.
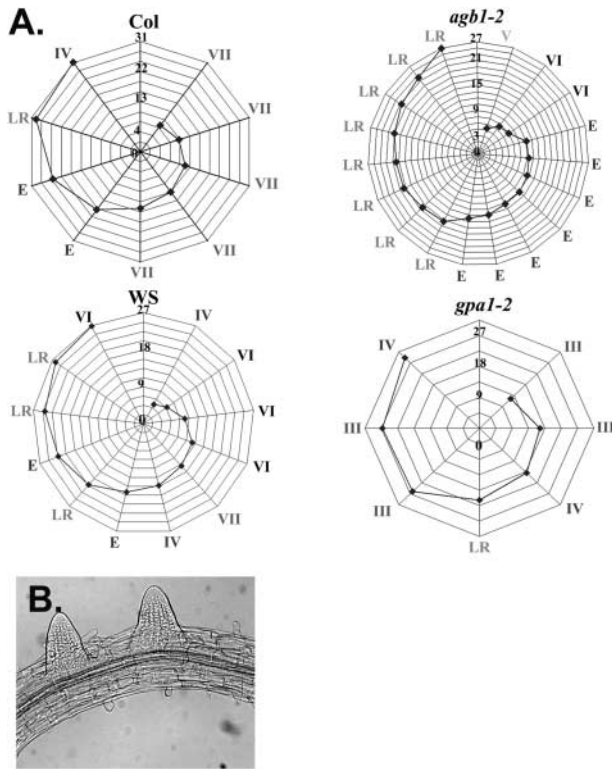
Figure 5. Lateral Root Primordia in the G Protein Mutants.

(A) Developmental stages of lateral root primordia as a function of position along the primary roots of 5-day-old, light-grown seedlings is shown for *agb1-2* and *gpa1-2* and their respective ecotypes, Columbia (Col) and Wassilewskija (WS). Developmental stages, indicated with roman numerals, are assigned according to Malamy and Benfey (1997). The center of each spider graph represents the tip of the primary root, and radially distal to the center is the position of the root-shoot junction. The distance from the root tip to the root-shoot junction (mm) is indicated along the radius. The density of primordia is represented visually by the density of threads in the web. The genotypes are indicated above each graph. E, emergent lateral root; LR, lateral root.

(B) Frequently, twinned primordia were observed in *agb1* roots but never in wild-type or *gpa1* roots.

tor. The loss of Gα results in an increase in free Gβγ and therefore more signal output, whereas the loss of Gβ decreases it. Gβ genetically acts downstream of Gα in the classic model, and because it does not undergo a conformational change, its activity is constitutive when released from the heterotrimeric complex via either Gα activation or the loss of Gα in the *gpa1* mutant. Alternatively, if Gα is the predominant signaling factor, similar phenotypes for both Gα and Gβ loss-of-function mutants are expected, because Gβ is required for the recruitment of Gα to the receptor for activation.

One possible explanation for the root phenotypes is that

loss-of-function mutations result in altered pool sizes of free auxin in roots. Application of the auxin transport inhibitor NPA reduces the number of lateral roots (Casimiro et al., 2001; Himanen et al., 2002). The mechanism may be disruption of the cycling of auxin transporters to the plasma membrane (Friml et al., 2002a, 2002b). Lateral root formation occurs in NPA-pretreated roots in an auxin dose-dependent manner, serving as a cell division assay for auxin sensitivity. Figure 6A illustrates this auxin dependence of root formation, because plants expressing a bacterial auxin lyase gene have fewer primary roots than control plants on auxin. Auxin-induced lateral root formation was quantitated in G protein mutants and transgenic lines. *agb1* primary roots form more lateral roots, whereas *gpa1* primary roots form fewer lateral roots, compared with their respective wild-type ecotypes (Figure 6B). Rescue of the AGB1 attenuation of auxin-induced roots to wild-type levels was demonstrated by genetically complementing the *agb1-2* mutant with a dexamethasone-inducible promoter to drive the expression of the *AGB1* cDNA (Figure 6B). The observation that both *agb1* and *gpa1* mutants respond to auxin, albeit with altered sensitivities, indicates that a G protein cannot directly couple the auxin signal to an effector, leading to cell division. In addition, these results suggest that the free Gβγ-subunit attenuates the auxin pathway (Figure 7A, hypothesis 1). The alternative view (Figure 7A, hypothesis 2), that Gα potentiates the auxin pathway, is less tenable because in the classic paradigm, Gβγ is required for Gα activation; therefore, in this scenario, the phenotype of Gα and Gβγ mutants would be the same for root cell division.

To distinguish between primary signaling by the Gα-subunit versus the released Gβγ-subunits, we examined the root phenotypes of plants that overexpress different forms of the Gα-subunits (GOX lines C3 and H2) and Gβ-subunits (BOX lines 6-4 and 8-3) and compared the observed phenotypes with the expectations based on the alternative hypotheses (Figure 7A). A dexamethasone-inducible promoter drove the expression of wild-type *GPA1* and *AGB1*, whereas constitutive expression of a mutant Gα (GPA1*) occurred using the viral 35S promoter (lines D and E). Controlled overexpression of a wild-type Gα should sequester, and therefore deplete Gβγ because in the absence of activation, the ground state of Gα is its GDP conformation. By contrast, GPA1*, as a result of a Q222L mutation disabling its GTPase activity, remains in its activated GTP conformation and should be unable to deplete the Gβγ pool. Although GPA1* is capable of constitutively activating its cognate effectors, it is unable to sequester Gβγ. This approach has been successful in distinguishing the predominant role of G protein subunits in *Drosophila* asymmetric cell division (Schaefer et al., 2001). The expression levels of two independent transformants of each G protein gene construct were quantitated, and the fold change over controls was determined (see supplemental data online). Plants that express wild-type *GPA1* by 6- to 10-fold have more roots than controls, mimicking the *agb1* phenotype, whereas GPA1* overexpression has no
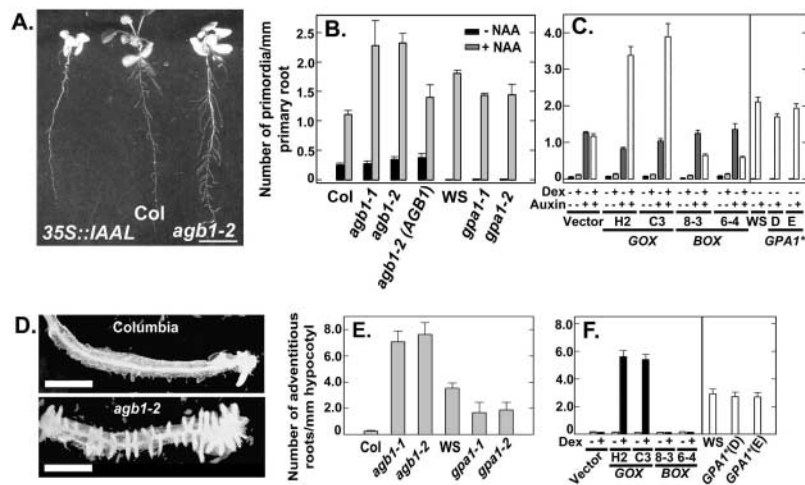
Figure 6. Lateral and Adventitious Root Development in G Protein Mutants.

(A) Seedlings were grown on 5 μM NPA for 9 days and transferred to auxin containing 1 × Murashige and Skoog (1962) salts supplemented with 1% Suc and grown for an additional 12 days under continuous light. *35S::IAAL* is a transgenic line constitutively expressing a bacterial IAA lyase gene that results in the breakdown of endogenous auxin. Col, Columbia. Bar = 10 mm.

(B) Lateral root primordia formation after transfer to auxin-containing plates. Seedlings were grown for 9 days on 5 μM NPA and transferred to plates containing auxin (+NAA) or not (−NAA) for an additional 96 h under continuous light on vertically oriented plates. Seedlings were cleared, and root primordia were counted using Nomarski optics. The standard error of the mean is based on 10 seedlings. *agb1-2 (AGB1)* is the genetically complemented *agb1-2* mutant. WS, Wassilewskija.

(C) Seedlings were grown as in **(B)** for 9 days. Seedlings were transferred to plates with or without 0.1 μM auxin and with or without 100 nM dexamethasone (Dex). The seedlings were cleared and counted as in **(B)**. Plants overexpressing *GPA1* are indicated as GOX lines C3 and H2, and plants overexpressing AGB1 are indicated as BOX lines 6-4 and 8-3. A dexamethasone-inducible promoter drove the expression of wild-type *GPA1* and *AGB1*, whereas constitutive expression of a mutant Gα (GPA1*) occurred using the viral 35S promoter (lines D and E). The standard error of the mean is based on 10 seedlings. The genotypes are indicated on the *x* axis.

(D) Adventitious root development on excised hypocotyl explants. Seedlings were grown axenically for 7 days in dim light (2 μmol·m^{-2}·s^{-1}). Excised hypocotyls were excised aseptically and transferred to plates containing 100 ng/mL 1-naphthylacetic acid. Plates were prepared according to the protocol of Kubo and Kakimoto (2000). Excised hypocotyls were grown for an additional 10 days under continuous light (65 μmol·m^{-2}·s^{-1}) and photographed. Bars = 2 mm.

(E) and **(F)** The total number of adventitious roots was divided by the length of the excised hypocotyls. The standard error of the mean is based on 10 excised hypocotyls. The genotypes are indicated.

effect on auxin-induced cell division in roots (Figure 6C). The inducible overexpression of *AGB1* causes fewer lateral roots compared with control, auxin-treated, primary roots.

Auxin treatment of hypocotyls produces roots adventitiously. To test the effect of gain and loss of G protein function in a tissue that lacks preexisting root primordia, we treated hypocotyl explants from mutant and wild-type seedlings with auxin (Figure 6D). As shown for lateral root formation, *agb1* hypocotyls were hypersensitive to auxin, whereas *gpa1* roots were less sensitive (Figure 6E). Hypocotyls overexpressing the wild-type form of *GPA1*, but not *GPA1**, were hypersensitive to auxin, and increased *AGB1* expression resulted in fewer roots than from control hypocotyls (Figure 6F). Altered auxin sensitivity depended on G protein subunit expression, because lateral roots did not form in the absence of dexamethasone.

These results are consistent with a model in which the Gβγ subunit negatively regulates auxin-induced cell division (Figures 7A and 7B), although a formal model must consider the possible role of autoregulation and its early timing, because root cell division does not become apparent for hours after auxin application. Therefore, changes in G protein levels were extrapolated from quantitative PCR data of *GPA1* and *AGB1* steady state message levels in the wild type and the mutants. Figure 8 shows that auxin causes an increase in *GPA1* message and a decrease in *AGB1* message within 15 min of application. The change is stable over at least 60 min. Neither the increase nor the decrease in steady state levels of the respective messages depended on a functional G protein complex, because the same changes in steady state message levels were observed in the corresponding G protein mutants.

The model shown in Figure 7C posits that the free Gβγ-subunit attenuates auxin-induced cell division. Accordingly, the Gα-subunit blocks Gβγ action by sequestering Gβγ into the heterotrimeric complex. Negative autoregulation of the

auxin path occurs in a G protein–independent manner via an increase in Gα and a decrease in Gβ mRNA steady state levels (Figure 8).

A Set of Genes Negatively Regulated by AGB1

To test the model shown in Figure 7C, we examined the gene expression profiles of wild-type and *agb1* seedlings treated with 10 μM auxin for 20 min. The rationale for this
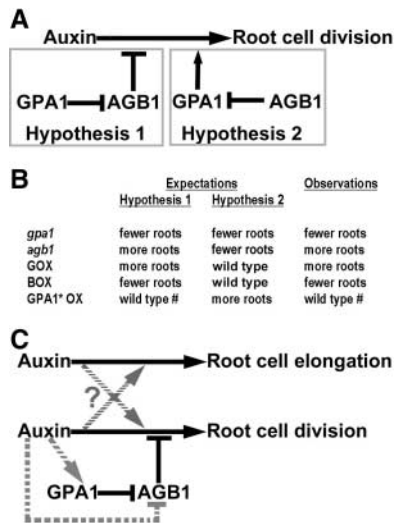

Figure 7. Hypotheses and Proposed Model for the Role of Heterotrimeric G Proteins in Auxin-Induced Lateral Root Development.

(A) Based on our observations, two possible hypotheses are proposed. In hypothesis 1, *AGB1* is expected to function downstream of *GPA1* and inhibits auxin-induced cell division during lateral root development, and *GPA1* inhibits *AGB1* function. In hypothesis 2, *GPA1* promotes auxin-induced cell division during lateral root development and functions downstream of *AGB1*, which inhibits *GPA1* function.

(B) Expectations and observations based on the proposed hypotheses. Overexpression of native GPA1 is expected to reduce the free AGB1 pool, whereas the activated Gα, GPA1*, is unable to sequester AGB1 (Schaefer et al., 2001).

(C) Favored model. In this model, auxin-induced cell elongation in roots is independent of the heterotrimeric G protein complex. Heterotrimeric G proteins modulate auxin-induced cell division during lateral root formation (lower black arrow), and this regulation is attenuated by the action of a Gβγ-subunit when it is released from the heterotrimeric complex. Because release is controlled by Gα activation, GPA1 formally inhibits AGB1 action. Negative feedback occurs via an auxin-induced decrease in the steady state level of *AGB1* transcript and an increase in *GPA1* transcript. The negative feedback loop operates independently of G proteins, because the same changes in the steady state level of transcript were found in the G protein mutants (see Figure 8). Because altered cell division can be compensated for by the corresponding change in cell elongation, cross-talk between the two competing pathways must occur.
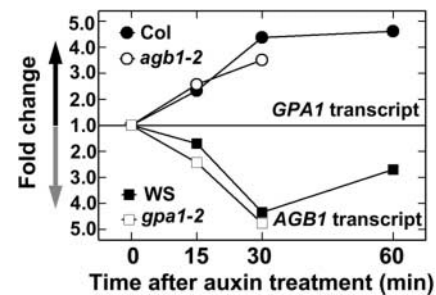

Figure 8. Auxin-Dependent *GPA1* and *AGB1* Transcript Levels in Wild-Type and Mutant Seedlings.

Total RNA from 5-day-old, dark-grown seedlings treated with 20 μM IAA for 0, 15, 30, or 60 min was used as a template for real-time PCR analysis. Normalized fold changes were calculated as described in Methods and the supplemental data online. Col, Columbia; WS, Wassilewskija.

experiment is that auxin rapidly alters the expression of a set of genes that function in concert in cell division, and we postulate that AGB1 acts upstream of this control of steady state levels of corresponding mRNAs. Strict criteria were established for the acceptance of genes into an auxin-induced gene set. For a gene to be scored as auxin regulated, its expression level must be at least 500 pixel units in controls for downregulated genes or in the auxin-treated samples for upregulated genes, and the change in expression between controls and treated seedlings must be at least twofold. Only 150 genes among 8300 analyzed met these criteria for auxin upregulation, and 114 genes met the criteria for auxin downregulation (see supplemental data online). These included most of the known auxin-regulated genes, such as *Aux/IAA*, *GH3*, *SAUR*s, and *GST*.

Additional criteria were established to determine if the expression of a set of genes was uncoupled in *agb1-2* seedlings. The level of expression in *agb1-2* in the absence of auxin must be within 25% of the expression level of the auxin-treated wild-type seedlings. Furthermore, the ratio of expression of a gene in auxin-treated *agb1-2* to control *agb1-2* seedlings must approximate 1. Forty-seven and 17 genes among the auxin-upregulated and -downregulated sets, respectively, met these criteria, indicating that approximately one-quarter of the auxin-regulated genes require AGB1 for correct basal expression. These 47 and 17 genes selected as uncoupled in *agb1* seedlings from auxin-upregulated and -downregulated sets, respectively, were clustered, and their expression was compared with that in wild-type seedlings (Figure 9). Although 30% of the genes had "unknown protein" annotations and 9% were reported previously to be regulated by auxin (see supplemental data online), most other genes identified here were informative and not shown previously to be regulated by auxin. Twenty percent of the genes encoded transcription factors and metabolic enzymes.
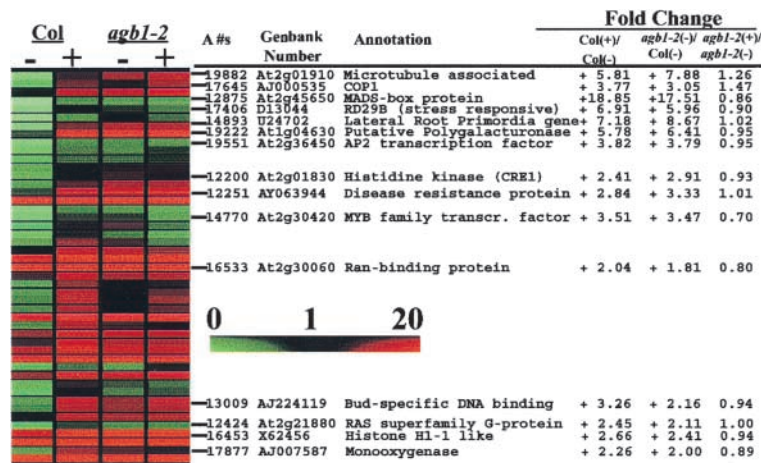
Col		agb1-2		A#s	Genbank Number	Annotation	Fold Change		
−	+	−	+				Col(+)/ Col(−)	agb1-2(−)/ Col(−)	agb1-2(+)/ agb1-2(−)
				19882	At2g01910	Microtubule associated	+ 5.81	+ 7.88	1.26
				17645	AJ000535	COP1	+ 3.77	+ 3.05	1.47
				12875	At2g45650	MADS-box protein	+18.85	+17.51	0.86
				17406	D13044	RD29B (stress responsive)	+ 6.91	+ 5.96	0.90
				14893	U24702	Lateral Root Primordia gene	+ 7.18	+ 8.67	1.02
				19222	At1g04630	Putative Polygalacturonase	+ 5.78	+ 6.41	0.95
				19551	At2g36450	AP2 transcription factor	+ 3.82	+ 3.79	0.95
				12200	At2g01830	Histidine kinase (CRE1)	+ 2.41	+ 2.91	0.93
				12251	AY063944	Disease resistance protein	+ 2.84	+ 3.33	1.01
				14770	At2g30420	MYB family transcr. factor	+ 3.51	+ 3.47	0.70
				16533	At2g30060	Ran-binding protein	+ 2.04	+ 1.81	0.80
				13009	AJ224119	Bud-specific DNA binding	+ 3.26	+ 2.16	0.94
				12424	At2g21880	RAS superfamily G-protein	+ 2.45	+ 2.11	1.00
				16453	X62456	Histone H1-1 like	+ 2.66	+ 2.41	0.94
				17877	AJ007587	Monooxygenase	+ 2.26	+ 2.00	0.89

Figure 9. Auxin Genes Upregulated and Derepressed in the *agb1-2* Mutant.

Total RNA from 2-day-old, dark-grown seedlings, treated with (+) or without (−) 10 μM IAA for 20 min, was hybridized to microarrays containing ~8300 Arabidopsis gene probe sets. A set of 47 AGB1-dependent, auxin-regulated genes was established based on the criteria described in the text, and the normalized expression is color coded, with a value of 1 (black) equal to the average expression on the chip. Values less (green) and more (red) than the chip average are indicated by the gradation of color. A#s represent Affymetrix identification numbers. Fold changes in expression are shown for different comparisons to illustrate that these are auxin-induced genes that are derepressed in the *agb1-2* mutant. Col(+)/ Col(−) represents the fold change induced by the auxin treatment, and similar values in the *agb1-2*(−)/Col(−) column indicate that the expression of the gene is derepressed in the *agb1-2* mutant. The fold change of ~1 for the *agb1-2*(+)/*agb1-2*(−) comparison indicates that auxin does not alter gene expression in the *agb1-2* mutant. Both the auxin-upregulated and -downregulated annotated gene sets with raw scores are provided in the supplemental data online.

The remaining genes involved G protein signaling, stress, and kinase functions (see supplemental data online). Several other genes in these sets are known to be involved in cell division, specifically lateral root development, but were not clustered previously as auxin regulated or known to require Gβ for basal repression. In addition, some of the known auxin-regulated genes are implicated here in cell division.

As an independent confirmation of the microarray data, expression levels of the *Lateral Root Primordia* (*LRP*) gene were tested using real-time PCR. By this method, *LRP* mRNA steady state levels in Columbia increased 12.6-fold (versus 7.2-fold by microarray) after the application of auxin. In untreated *agb1-2* seedlings, *LRP* mRNA steady state levels were 7.3-fold (versus 8.7-fold by microarray) greater than untreated Columbia seedlings, in close agreement with the microarray results and consistent with our conclusion that a set of auxin-regulated genes are deregulated in the *agb1-2* mutant.

DISCUSSION

Auxin comprises a class of plant growth regulators that act as morphogens to direct two competing cellular actions depending on the concentration. At a low auxin concentration, cells arrest at G1 and expand, whereas at a slightly higher concentration, cells proceed to G2/M and divide, followed by minimal expansion to recharge the meristematic cell volume. Root formation is a model system in which to study the relationship between these two auxin pathways. Root primordia form by orchestrated cell division of three competent cells in the subtending pericycle, and the root emerges from its associated ground tissue by elongation (Malamy and Benfey, 1997; Beeckman et al., 2001; Dubrovsky et al., 2001). In root formation, both cell division and elongation are controlled strictly by auxin. Although a number of auxin-resistant mutants have root phenotypes, the *alf4-1* mutation is especially informative because primary roots in this mutant fail to make lateral roots yet retain auxin sensitivity, providing evidence for at least two separable auxin signaling pathways (Celenza et al., 1995). Studies on the role of the NAM/CUC transcriptional regulator NAC1 also support two separable auxin pathways in root formation (Xie et al., 2000). The expression of NAC1 is auxin induced and most striking in developing root primordia, although it is present in other tissues (Xie et al., 2002). Antisense cosuppression of NAC1 resulted in fewer lateral roots yet had no effect on cell elongation in the primary root.

It is not known whether the initial perception of auxin occurs via two (or more) receptors that control these separable responses or whether multivalent occupancy of a single receptor activates the two pathways individually. In Arabidopsis, Auxin Binding Protein1 (ABP1) is essential for cell elon-

gation but not for cell division (Chen et al., 2001); thus, the former possibility is favored at present. We previously showed that cell division, likely initiated by auxin, is altered in *gpa1* mutants; therefore, we proposed that a heterotrimeric G protein is involved in plant cell proliferation (Ullah et al., 2001). We extend that work here to show that although auxin-induced cell division does not require a G protein for direct coupling, the sensitivity toward auxin is regulated by a pathway that involves a heterotrimeric G protein. Moreover, we conclude that the Gβ-subunit released from the heterotrimeric complex operates to attenuate auxin signaling upstream of auxin's control of mRNA steady state levels (Figure 8C). This conclusion is tempered by the assumption that the classic paradigm for heterotrimeric G protein coupling operates similarly in Arabidopsis. However, analysis of the double mutant between *agb1-2* and new null alleles of *gpa1* in the Columbia ecotype (*gpa1-3* and *gpa1-4*) support this conclusion (data not shown). Double mutants have the lateral root phenotype of the single *agb1-2* mutant. The genotype and partial characterization of the new *gpa1* alleles and the double mutant are described in Jones et al. (2003).

It also is possible that Gβγ serves as a positive regulator of cell elongation in the roots, because *agb1* roots are shorter than wild-type roots under certain conditions, and seedlings that inducibly express AGB1 conditionally have longer roots than wild-type seedlings (data not shown). These ideas may seem at variance with our data (see supplemental data online) that the sensitivity to auxin inhibition of root growth is wild type in the G protein mutants; however, auxin-induced growth and auxin-inhibited growth may be separate pathways. Alternatively, AGB1 could promote cell elongation independently of auxin.

In yeast, the mechanism of Gβγ action classically defined by the pheromone response in mating is partially known. The released Gβγ (Ste4/18p) interacts with the protein kinase (Ste20p) to cause a conformational change that enables Ste20p to phosphorylate the mitogen-activated protein kinase kinase kinase, Ste11p (van Drogen et al., 2001). One possibility is that Gβγ recruits the mitogen-activated protein kinase cascade scaffold (Ste5p) to the plasma membrane, bringing the tethered Ste11p into proximity to Ste20p (Pryciak and Huntress, 1998). Interestingly, auxin action via the mitogen-activated protein kinase pathway in Arabidopsis results in negative transcriptional regulation (Kovtun et al., 1998; Mockaitis and Howell, 2000), consistent with our findings here using the Gβ loss-of-function mutant. In addition, the plant mitogen-activated protein kinases are expressed in mitotic cells, suggesting their involvement in division (Bogre et al., 2000). Thus, at present, auxin signaling appears to share some similarity with the framework of the pheromone pathway in yeast.

In mammals, Gβγ coupling to effectors also occurs, and a well-understood pathway is Gβγ control of potassium inward conductance channels (Clapham and Neer, 1997; Corey and Clapham, 2001). In Arabidopsis, the G protein couples abscisic acid's negative control of potassium flux (Wang et al., 2001), but it is not known if this involves Gβγ interaction with the channel directly, if Gα is the predominant interacting subunit, or if an alternative effector is activated. Potassium flux is critical for auxin-induced cell elongation (Thiel et al., 1993; Blatt and Thiel, 1994; Philippar et al., 1999), and a direct test of whether auxin-regulated potassium flux occurs in the G protein mutants is warranted.

Gene expression profiling revealed several informative examples of genes shown to be derepressed in *agb1-2*. One of these is *LRP1*. *LRP1* encodes a novel protein that is expressed in the dividing cells at or before stage II (Smith and Fedoroff, 1995), and its expression is induced rapidly by auxin in the wild type (Figure 9). Additional genes now have been implicated in the auxin signaling pathway and shown to be repressed by a G protein–dependent pathway. The expression of *COP1* increases nearly fourfold with auxin application in wild-type seedlings, but *COP1* is expressed constitutively in the *agb1* mutant (Figure 9). *cop1* mutants share some of the de-etiolated phenotypes seen in *agb1*, such as short hypocotyls and open hooks (Schwechheimer et al., 2000), and it is interesting that COP1 is predicted to have a β-propeller structure like that shown here for AGB1.

AGB1 most likely couples another signal to modulate auxin action upstream of its transcriptional control, but the identity of that signal is not yet known. Considering the recent evidence suggesting that brassinosteroid signaling is coupled by a heterotrimeric G protein in Arabidopsis (Ullah et al., 2002) and the well-known observation that brassinosteroid and auxin signaling interact (Clouse, 1998; Ephritikhine et al., 1999; Yin et al., 2002), we propose that brassinosteroids fulfill this role.

METHODS

Molecular Modeling

The sequences of GPA1, AGB1, and AGG1 from *Arabidopsis thaliana* were submitted to four different fold-recognition World Wide Web servers to identify structural templates for homology modeling. The fold-recognition servers used were BIOINBGU (www.cs.bgu.ac.il/~bioinbgu/), 3D-PSSM (www.sbg.bio.ic.ac.uk/3dpssm/), GenTHREADER (bioinf.cs.ucl.ac.uk/psipred/index.html), and FUGUE (www-cryst.bioc.cam.ac.uk/~fugue/prfsearch.html). The fold-recognition servers identified GPA1, AGB1, and AGG1 as Gα, Gβ, and Gγ proteins, respectively. Alignments between the Arabidopsis sequences and several different structural templates of G proteins were provided by the servers. These alignments varied in detail among the different servers, although all servers recognized these proteins as G proteins. The CLUSTAL X program (Thompson et al., 1997) was used to align 119 Gα sequences (including GPA1 from Arabidopsis) obtained from the SWISS-PROT protein sequence database (Bairoch and Apweiler, 2000) with the mammalian sequence from the structure 1GOT (Protein Data Bank accession code) obtained from the Protein Data Bank (www.rcsb.org).

A consensus alignment between the Arabidopsis sequence and the mammalian Gα in 1GOT was determined by comparing the alignments from the different fold-recognition servers with the multiple sequence alignment from CLUSTAL X. A model of GPA1 was

built using the Modeler module of the Insight II molecular modeling system from Accelrys, Inc. (www.accelrys.com). The homology model was evaluated for sequence-structure compatibility using the Verify function of the Profiles-3D module of Insight II. Different alignments between GPA1 and the Gα protein from 1GOT were generated in regions that had low Profiles-3D/Verify scores. A new homology model was generated from each new alignment and again evaluated for structure-sequence compatibility. This was an iterative process that continued until the compatibility between sequence and structure could not be improved. A similar methodology was followed for the modeling of AGB1 and AGG1. In the case of AGB1, 29 Gβ sequences were obtained from SWISS-PROT and aligned with the Gβ sequence from 1GOT. Twenty-seven Gγ sequences were obtained from SWISS-PROT and aligned with the Gγ sequence from 1GOT. A similar iterative process was used to generate homology models for AGB1 and AGG1.

CLUSTAL X was used to generate quality scores ranging from 0 to 100 to represent the conservation of each position in the multiple sequence alignment. A score of 100 represents a position in the alignment that is invariant, and a score of 0 represents a position that is highly variant among all of the individual sequences. The calculation of the quality score is dependent on a residue comparison matrix giving a score for the alignment of two residues. The quality score for a position is defined as the mean of the sequence distances between each sequence and the consensus position according to the residue comparison matrix. Scores were output to a text file for every position in the multiple sequence alignment where there was a residue (not a gap) in the Arabidopsis sequence. CLUSTAL X also labels positions in the alignment window using various symbols: an asterisk (*) for positions that are invariant, a colon (:) for highly conserved positions, and a dot (.) for conserved positions. This labeling generally corresponds to a given range of quality scores, but not always. For example, a particular position in the Gβ alignment had 24 Thr residues and 6 Ser residues. The score for this position was 78 (a score lower than those for some positions that were not labeled as highly conserved), but the residue was reasonably labeled as highly conserved (:) in the sequence window because the residue in that position was always a Ser or a Thr. We designated positions in the alignment as (1) highly conserved, (2) conserved, or (3) not conserved based on a combination of two criteria. Positions in the alignment were highly conserved if the quality score was ≥80, conserved if the quality score was ≥40 but <80, and not conserved if the score was <40. If the labeling (: and .) in the alignment window indicated that a position was considered more conserved than was determined by the quality score, the position was upgraded. The alignments used to calculate the quality scores were the multiple sequence alignments generated for the homology modeling. All figures were created with SPOCK (Christopher, 1998).

Isolation of the *agb1-2* Mutant and Genetic Complementation

DNA from 40,000 T-DNA insertion lines in the Columbia ecotype were screened by PCR using a primer 200 bp downstream of the *AGB1* stop codon in the 3′ untranslated region (5′-AGTAGCGTG-TTGAAGCAGTTTAGTTCCC-3′) and a T-DNA left border primer (5′-GGCAATCAGCTGTTGCCCGTCTCACTGGTG-3′). A single insertion in the fourth exon of *AGB1* was isolated, and the insertion was confirmed by sequencing. Genetic complementation was accomplished by transforming *agb1-2* plants with a dexamethasone-inducible *AGB1* cDNA and assaying for lateral root primordia as described

below except that the roots developed in the presence of 0.1 μM dexamethasone.

Mutant Characterization and Cell Division and Elongation Assays

Mature plants were grown under a short-day (8-h-light/16-h-dark) regimen at 23°C for 3 weeks and then transferred to a long-day (16-h-light/ 8-h-dark) regimen for an additional 2 weeks. Mature roots were scored from plants grown under similar conditions. Special care was taken to ensure that no lateral root was lost during soil removal. Siliques were collected from fully mature plants (∼8 weeks old).

Plants were grown for 2 days in darkness for hypocotyl and epidermal cell length measurements. Hypocotyls of dark-grown seedlings were incubated in chloral hydrate (2.5 g/mL) for 24 h to clear the tissue and then examined using Nomarski optics. Digital images of cells were analyzed for area and length using NIH Image 1.61 software. Five hypocotyls were measured, and data are presented as means ± SE.

For histological analyses, 2-day-old dark-grown seedlings were fixed in Karnovsky solution (4% paraformaldehyde, 2.5% glutaraldehyde, and 0.1 M cacodylate buffer) for 24 h at 4°C, dehydrated in an ethanol series, and embedded in paraffin. Seedlings were sectioned at 10-μm thickness and stained with Safranin O and Fast Green. Developmental stages of the chloral hydrate–cleared lateral root primordia depicted in Figure 5 were determined from 5-day-old roots grown under continuous light at 23°C. Quantitation of lateral roots and primordia as depicted in Figure 6A was performed using roots grown on 5 μM naphthylphthalamic acid for 9 days and transferred to 0.1 μM auxin containing 1 × Murashige and Skoog (1962) salts supplemented with 1% Suc and grown vertically under continuous light. The plates were supplemented with or without 100 nM dexamethasone for BOX, GOX, and vector lines. After clearing, primordia were counted using Nomarski optics. The standard error of the mean is based on 10 seedlings. Adventitious roots, as depicted in Figures 6D to 6F, were measured according to the protocols of Kubo and Kakimoto (2000). Seedlings were grown for 7 days in dim light (2 μmol·m^{-2}·s^{-1}). Hypocotyls were excised aseptically and transferred to plates containing 100 ng/mL 1-naphthyl-acetic acid. Excised hypocotyls were grown for an additional 10 days under continuous light (65 μmol·m^{-2}·s^{-1}) and then scored with a dissecting microscope for the number of adventitious roots per length of hypocotyl. The standard error of the mean is based on 10 excised hypocotyls.

Construction of GOX, BOX, and GPA1* Lines

The full-length Arabidopsis *GPA1* and *AGB1* cDNA coding regions were cloned into binary vector pTA7002 (Aoyama and Chua, 1997) for *Agrobacterium tumefaciens*–mediated transformation of Columbia and *agb1-2*. GPA1* was made by replacing A with T at position 1264 of *GPA1* by site-directed mutagenesis (Kroll et al., 1992) to create a Q-to-L change. The mutated cDNA was cloned into pGPTV-HYG vector. The vector was introduced into Agrobacterium strain GV3101 for plant transformation.

High-Throughput Phenotype Profiling

Details of the Paradigm Genetics Phenotypic Analysis Platform have been described previously (Boyes et al., 2001). The analysis of ger-

mination and seedling development was conducted on plants grown on Petri plates containing 0.5 × Murashige and Skoog (1962) salts that were oriented vertically within growth chambers. In this configuration, the roots grow over the surface of the agar and are readily visible. Soil-grown plants were used for the characterization of the later stages of development. In all cases, plants were grown under a 16-h daylength, with day and night temperatures of 22 and 20°C, respectively. Data for seed and rosette area, perimeter, major axis, minor axis, standard deviation of the radius, and eccentricity were derived from digital image analysis using IP Lab software (Scanalytics, Fairfax, VA). All other data were collected by visual inspection or using standard measuring devices, including analytical balances, calipers, and rulers.

Gene Expression Profiling

Three samples of seedlings were grown for 2 days in darkness in liquid culture (1 × Murashige and Skoog [1962] medium and 1% Suc) and treated with 10 μM indole-3-acetic acid for 20 min. Total RNA was isolated from the pooled samples three times using the Plant RNAeasy Kit (Qiagen, Santa Clarita, CA) according to the manufacturer's protocol, and the RNA was pooled. Purified RNA (7 μg) was reverse transcribed by Superscript II reverse transcriptase (Life Technologies, Grand Island, NY) using T7-(dT)$_{24}$ primer containing a T7 RNA polymerase promoter. After synthesis of the second strand, this product was used in in vitro transcription to generate biotinylated complementary RNA. Fragmented complementary RNA was hybridized to an Affymetrix Arabidopsis Genome Array Genechip (Santa Clara, CA) according to the manufacturer's protocol. This high-density oligonucleotide-based array contains ~8300 Arabidopsis gene probe sets and >100 EST clusters selected from the NCBI GenBank database. Each microarray was used to assay a single sample. After hybridization, the microarray was washed and stained on an Affymetrix fluidics station and scanned with the Hewlett-Packard GeneArray Scanner (Boise, ID). Affymetrix GeneChip Microarray suite 4.0 software was used for basic analysis. The whole procedure was performed at the Genomics Core and Microarray Facility at the University of North Carolina at Chapel Hill. Data analysis was performed with Genespring software version 6.04 (Silicon Genetics, San Carlos, CA).

Expression was normalized to the median value for the entire raw data set of the corresponding chip. To calculate fold changes and not lose genes that are not expressed in one sample but are switched on in the other, or vice versa, we set the lowest raw data value at an arbitrary 10. To eliminate "fold-change" calls within the range of background noise, we required that genes classified as "upregulated" have raw data values of at least 500 and genes classified as "downregulated" have raw data values of at least 500 in the control (Hoffmann et al., 2001). Within these strict parameters, the genes selected were either upregulated or downregulated at least twofold in treatments compared with the controls. The entire raw score data set is provided in the supplemental data online.

RNA Quantitation by Real-Time PCR

Total RNA from different transgenic lines was isolated from seedlings grown in light for 10 days with or without 100 nM dexamethasone. Five hundred nanograms of total RNA was processed directly into cDNA by reverse transcription with Superscript II (Life Technologies) according to the manufacturer's protocol in a total volume of 20 μL.

One microliter of cDNA was used as a template for real-time PCR analysis. Oligonucleotides were synthesized by Sigma-Genosys (Woodlands, TX) using published sequence data from the NCBI database. The primer sequences were as follows: *GPA1*RT.FW, 5′-AGAAGTTTGAGGAGTTATATTACCAG-3′; *GPA1*RT.RV, 5′-AAGGCC-AGCCTCCAGTAA-3′; *AGB1*RT.FW, 5′-GACGTACTCGGGTGA-GCTT-3′; and *AGB1*RT.RV, 5′-GAGCATTCCACACGATTAAT-3′. The primers were selected from the 3′ site of the gene to ensure the availability of transcripts from oligo(dT)-based reverse transcription. The primers were expected to produce ~150-bp products. We used primers for a genomic marker, MYN21c, on the fifth exon of the Suc cleavage protein–like gene as a control to normalize the expression data for each gene. The sequences for the control primers are as follows: MYN21cF, 5′-CTAGCTTTGGAGTAAAAAGATTTGAGTGTG-CAACC-3′; and MYN21cR, 5′-TCTTTTCGCTGTTTAATTGTAACC-TTTGTTCTCGA-3′. They are expected to produce a product of 333 bp from the control gene. PCR amplification and fluorescence detection were accomplished using the Smart Cycler system from Cepheid, Inc. (Sunnyvale, CA). SYBR green was used as the intercalating dye. The thermal cycling conditions were as follows: 5 min in 96°C, followed by 40 cycles of 95°C for 15 s, 60°C for 15 s, and 72°C for 15 s. The "primary cycle threshold" values were used to calculate differences in fold changes between treatment and control samples.

As an independent confirmation of the microarray data, expression levels of the *Lateral Root Primordia* (*LRP*) gene were tested using real-time PCR. Two micrograms of total RNA from the same total RNA pool used for microarray analysis was used for cDNA synthesis. The primer sequences were as follows: LRP1FW, 5′-CGTGTCAAG-ACTGTGGAAATCAG-3′; and LRP1RV, 5′-AGGTCGAAAGAGACG-AGCCA-3′.

Upon request, all novel materials described in this article will be made available in a timely manner for noncommercial research purposes.

REFERENCES

Aharon, G.S., Snedden, W.A., and Blumwald, E. (1998). Activation of a plant plasma membrane Ca^{2+} channel by TGa1, a heterotrimeric G protein α-subunit homologue. FEBS Lett. **424,** 17–21.

Aoyama, T., and Chua, N.H. (1997). A glucocorticoid-mediated transcriptional induction system in transgenic plants. Plant J. **11,** 605–612.

Assmann, S.M. (2002). Heterotrimeric and unconventional GTP binding proteins in plant cell signaling. Plant Cell **14** (suppl.), S355–S373.

Bairoch, A., and Apweiler, R. (2000). The SWISS-PROT protein sequence database and its supplement TrEMBL in 2000. Nucleic Acids Res. **28,** 45–48.

Beeckman, T., Burssens, S., and Inze, D. (2001). The peri-cell-cycle in Arabidopsis. J. Exp. Bot. **52,** 403–411.

Beffa, R., Szell, M., Meuwly, P., Pay, A., Vogeli-Lange, R., Metraux, J.-P., Neuhaus, G., Meins, F., and Nagy, F. (1995). Cholera toxin elevates pathogen resistance and induces pathogenesis-related gene expression in tobacco. EMBO J. **14,** 5753–5761.

Blakely, L.M., Blakely, R.M., Colowit, P.M., and Elliot, D.S. (1988). Experimental studies on lateral root formation in radish seedling roots: Analysis of the dose-response to exogenous auxin. Plant Physiol. **87,** 414–419.

Blatt, M.R., and Thiel, G. (1994). K$^+$ channels of stomatal guard cells: Bimodal control of the K$^+$ inward-rectifier evoked by auxin. Plant J. **5,** 55–68.

Boerjan, W., Cervera, M.T., Delarue, M., Beeckman, T., Dewitte, W., Bellini, C., Caboche, M., Van Onckelen, H., Van Montagu, M., and Inze, D. (1995). Superroot, a recessive mutation in Arabidopsis, confers auxin overproduction. Plant Cell **7,** 1405–1419.

Bogre, L., Meskiene, I., Herberle-Bors, E., and Hirt, H. (2000). Stressing the role of MAP kinases in mitogenic stimulation. Plant Mol. Biol. **43,** 705–718.

Boyes, D.C., Zayed, A.M., Ascenzi, R., McCaskill, A.J., Hoffman, N.E., Davis, K., and Gorlach, J. (2001). Growth stage–based phenotypic analysis of Arabidopsis: A model for high throughput functional genomics in plants. Plant Cell **13,** 1499–1510.

Casimiro, I., Marchant, A., Bhalerao, R.P., Beeckman, T., Dhooge, S., Swarup, R., Graham, N., Inze, D., Sandberg, G., Casero, P.J., and Bennett, M. (2001). Auxin transport promotes Arabidopsis lateral root initiation. Plant Cell **13,** 843–852.

Celenza, J.L., Grisafi, P.L., and Fink, G.R. (1995). A pathway for lateral root formation in *Arabidopsis thaliana*. Genes Dev. **9,** 2131–2142.

Chen, J.-G., Ullah, H., Young, J.C., Sussman, M.R., and Jones, A.M. (2001). ABP1 is required for organized cell elongation and division in Arabidopsis embryogenesis. Genes Dev. **15,** 902–911.

Christopher, J.A. (1998). The Structural Properties Observation and Calculation Kit. (College Station, TX: The Center for Macromolecular Design, Texas A&M University).

Clapham, D.E., and Neer, E.J. (1997). G protein βγ subunits. Annu. Rev. Pharmacol. Toxicol. **37,** 167–203.

Clouse, S.D. (1998). Brassinosteroid affects the rate of cell division in isolated leaf protoplasts from *Petunia hybrida*. Plant Cell Rep. **17,** 921–924.

Corey, S., and Clapham, D.E. (2001). The stoichiometry of G_{bg} binding to G protein-regulated inwardly rectifying K$^+$ channels (GIRKs). J. Biol. Chem. **276,** 11409–11413.

Dubrovsky, J.G., Rost, T.L., Colon-Carmona, A., and Doener, P. (2001). Early primordium morphogenesis during lateral root initiation in *Arabidopsis thaliana*. Planta **214,** 30–36.

Ephritikhine, G., Fellner, M., Vannini, C., Lapous, D., and Barbier-Brygoo, H. (1999). The *sax1* dwarf mutant of *Arabidopsis thaliana* shows altered sensitivity of growth responses to abscisic acid, auxin, gibberellins and ethylene and is partially rescued by exogenous brassinosteroid. Plant J. **18,** 303–314.

Fairley-Grenot, K., and Assmann, S.M. (1991). Evidence for G protein regulation of inward K$^+$ channel current in guard cells of fava bean. Plant Cell **3,** 1037–1044.

Fischer, D. (2000). Hybrid fold recognition: Combining sequence derived properties with evolutionary information. Pac. Symp. Biocomput. **2000,** 119–130.

Friml, J., Benkova, E., Blilou, I., Wisniewska, J., Hamann, T., Ljung, K., Woody, S., Sandberg, G., Scheres, B., Jurgens, G., and Palme, K. (2002a). AtPIN4 mediates sink-driven auxin gradients and root patterning in Arabidopsis. Cell **108,** 661–673.

Friml, J., Wisniewska, J., Benkova, E., Mendgens, K., and Palme, K. (2002b). Lateral relocation of auxin efflux regulator PIN3 mediates tropism in Arabidopsis. Nature **415,** 806–809.

Gray, W.M., Ostin, A., Sandberg, G., Romano, C.P., and Estelle, M. (1998). High temperature promotes auxin-mediated hypocotyl elongation in Arabidopsis. Proc. Natl. Acad. Sci. USA **95,** 7197–7202.

Himanen, K., Boucheron, E., Vanneste, S., de Almeida Engler, J., Inzé, D., and Beeckman, T. (2002). Auxin-mediated cell cycle activation during early lateral root initiation. Plant Cell **14,** 2339–2351.

Hobbie, L., and Estelle, M. (1995). The *axr4* auxin-resistant mutants of *Arabidopsis thaliana* define a gene important for root gravitropism and lateral root initiation. Plant J. **7,** 211–220.

Hoffmann, W.K., deVos, S., Tsukaski, K., Wachsman, W., Pinkus, G.S., Said, J.W., and Koeffler, H.P. (2001). Altered apoptosis pathways in mantle cell lymphoma detected by oligonucleotide microarray. Blood **98,** 787–794.

Jones, A.M. (2002). G protein-coupled signaling in Arabidopsis. Curr. Opin. Plant Biol. **5,** 402–407.

Jones, A.M., Ecker, J.R., and Chen, J.-G. (2003). A re-evaluation of the role of the heterotrimeric G protein in coupling light responses in Arabidopsis. Plant Physiol., in press.

Jones, D.T. (1999). GenTHREADER: An efficient and reliable protein fold recognition method for genomic sequences. J. Mol. Biol. **287,** 797–815.

Jones, H.D., Smith, S.J., Desikan, R., Plakidou-Dymock, S., Lovegrove, A., and Hooley, R. (1998). Heterotrimeric G proteins are implicated in gibberellin induction of amylase gene expression in wild oat aleurone. Plant Cell **10,** 245–254.

Kelley, L.A., MacCallum, R.M., and Sternberg, M.J.E. (2000). Enhanced genome annotation using structural profiles in the program 3D-PSSM. J. Mol. Biol. **299,** 499–520.

Klee, H.J. (1987). The effects of overproduction of two *Agrobacterium tumefaciens* T-DNA auxin biosynthesis gene products in transgenic petunia plants. Genes Dev. **1,** 86–96.

Kovtun, Y., Chiu, W.-L., Zeng, W., and Sheen, J. (1998). Suppression of auxin signal transduction by a MAPK cascade in higher plants. Nature **395,** 716–720.

Kroll, S.D., Chen, J., De Vivo, M., Carty, D.J., Buku, A., Premont, R.T., and Iyengar, R. (1992). The Q205L Go-alpha subunit expressed in NIH-3T3 cells induces transformation. J. Biol. Chem. **267,** 23183–23188.

Kubo, M., and Kakimoto, T. (2000). The cytokinin-hypersensitive genes of Arabidopsis negatively regulate the cytokinin-signaling pathway for cell division and chloroplast development. Plant J. **23,** 385–394.

Lambright, D.G., Sondek, J., Bohm, A., Skiba, N.P., Hamm, H.E., and Sigler, P.B. (1996). The 2.0 A crystal structure of a heterotrimeric G protein. Nature **379,** 311–319.

Laskowski, M.J., Williams, M.E., Nusbaum, H.C., and Sussex, I.M. (1995). Formation of lateral root meristems is a two-stage process. Development **121,** 3303–3310.

Lease, K.A., Wen, J., Li, J., Doke, J.T., Liscum, E., and Walker, J.C. (2001). A mutant Arabidopsis heterotrimeric G protein β subunit affects leaf, flower, and fruit development. Plant Cell **13,** 2631–2641.

Malamy, J., and Benfey, P. (1997). Organization and cell differentiation in lateral roots of *Arabidopsis thaliana*. Genes Dev. **124,** 33–44.

Mason, M.G., and Botella, J.R. (2000). Completing the heterodimer: Isolation and characterization of an *Arabidopsis thaliana* G protein γ-subunit cDNA. Proc. Natl. Acad. Sci. USA **97,** 14784–14788.

Mockaitis, K., and Howell, S.H. (2000). Auxin induces mitogenic activated protein kinase (MAPK) activation in roots of Arabidopsis seedlings. Plant J. **24,** 785–796.

Muday, G.K., and Haworth, P. (1994). Tomato root growth, gravitropism, and lateral development: Correlation with auxin transport. Plant Physiol. Biochem. **32,** 193–203.

Murashige, T., and Skoog, F. (1962). A revised medium for rapid growth and bioassays with tobacco tissue culture. Physiol. Plant. **15,** 473–497.

Neuhaus, G., Bowler, C., Kern, R., and Chua, N.-H. (1993). Calcium/calmodulin-dependent and -independent phytochrome signal transduction pathways. Cell **73,** 937–952.

Philippar, K., Fuchs, I., Luthen, H., Hoth, S., Bauer, C.S., Haga, K., Thiel, G., Sandberg, G., Bottger, M., Becker, D., and Hedrich, R. (1999). Auxin-induced K$^+$ expression represents an essential step in coleoptile growth and gravitropism. Proc. Natl. Acad. Sci. USA **96,** 12186–12191.

Pryciak, P.M., and Huntress, F.A. (1998). Membrane recruitment of the kinase cascade scaffold Ste5p by the G beta gamma complex underlies activation of the yeast pheromone response pathway. Genes Dev. **12,** 2684–2697.

Schaefer, M., Petroncki, M., Dorner, D., Forte, M., and Knoblich, J.A. (2001). Heterotrimeric G proteins direct two modes of asymmetric cell division in the *Drosophila* nervous system. Cell **107,** 183–194.

Schwechheimer, C., and Deng, X.W. (2000). The COP/DET/FUS proteins: Regulators of eukaryotic growth and development. Semin. Cell Dev. Biol. **11,** 495–503.

Shi, J., Blundell, T.L., and Mizuguchi, K. (2001). FUGUE: Sequence-structure homology recognition using environment-specific substitution tables and structure-dependent gap penalties. J. Mol. Biol. **310,** 243–257.

Smith, D., and Fedoroff, N.V. (1995). *LRP1*, a gene expressed in lateral and adventitious root primordia of Arabidopsis. Plant Cell **7,** 735–745.

Thiel, G., Fricker, M.R., White, I.R., and Millner, P. (1993). Modulation of K$^+$ channels in *Vicia* stomatal guard cells by peptide homologs to the auxin-binding protein C terminus. Proc. Natl. Acad. Sci. USA **90,** 11493–11497.

Thompson, J.D., Gibson, T.J., Plewniak, F., Jeanmougin, F., and Higgins, D.G. (1997). The ClustalX Windows interface: Flexible strategies for multiple sequence alignment aided by quality analysis tools. Nucleic Acids Res. **24,** 4876–4882.

Timpte, C., Lincoln, C., Pickett, F.B., Turner, J., and Estelle, M. (1995). The *AXR1* and *AUX1* genes of Arabidopsis function in separate auxin-response pathways. Plant J. **8,** 561–569.

Ueguchi-Tanaka, M., Fujisawa, Y., Kobayashi, M., Ashikari, M., Iwasaki, Y., Kitano, H., and Matsuoka, M. (2000). Rice dwarf mutant *d1*, which is defective in the α subunit of the heterotrimeric G protein, affects gibberellin signal transduction. Proc. Natl. Acad. Sci. USA **97,** 11638–11643.

Ullah, H., Chen, J.-G., Wang, S., and Jones, A.M. (2002). Role of a heterotrimeric G protein in regulation of Arabidopsis seed germination. Plant Physiol. **129,** 897–907.

Ullah, H., Chen, J.-G., Young, J.C., Im, K.-H., Sussman, M.R., and Jones, A.M. (2001). Modulation of cell proliferation by heterotrimeric G protein in *Arabidopsis*. Science **292,** 2066–2069.

Vanderbeld, B., and Kelly, G.M. (2000). New thoughts on the role of beta-gamma subunit in G protein signal transduction. Biochem. Cell Biol. **78,** 537–550.

van Drogen, F., Stuke, V.M., Jorritsma, G., and Peter, M. (2001). MAP kinase dynamics in response to pheromones in budding yeast. Nat. Cell Biol. **3,** 1051–1061.

Wall, M.A., Coleman, D.E., Lee, E., Iniguez-Lluhi, J.A., Posner, B.A., Gilman, A.G., and Sprang, S.R. (1995). The structure of the G protein heterotrimer Gi$_{a1b1g1}$. Cell **83,** 1047–1058.

Wall, M.A., Posner, B.A., and Sprang, S.R. (1998). Structural basis of activity and subunit recognition in G protein heterotrimers. Structure **6,** 1169–1183.

Wang, X.-Q., Ullah, H., Jones, A.M., and Assmann, S.M. (2001). G protein regulation of ion channels and abscisic acid signaling in *Arabidopsis* guard cells. Science **292,** 2070–2072.

Warpeha, K.M.F., Hamm, H.E., Rasenick, M.M., and Kaufman, L.S. (1991). A blue-light activated GTP-binding protein in the plasma membrane of etiolated peas. Proc. Natl. Acad. Sci. USA **88,** 8925–8929.

Wise, A., Thomas, P.G., Carr, T.H., Murphy, G.A., and Millner, P.A. (1997). Expression of the Arabidopsis G protein GPa1: Purification and characterization of the recombinant protein. Plant Mol. Biol. **33,** 723–728.

Xie, Q., Frugis, G., Colgan, D., and Chua, N.-H. (2000). Arabidopsis NAC1 transduces auxin signal downstream of TIR1 to promote lateral root development. Genes Dev. **14,** 3024–3036.

Xie, Q., Guo, H.-S., Dallman, G., Fang, S., Weismann, A.M., and Chua, H.-H. (2002). SINAT5 promotes ubiquitin-related degradation of NAC1 to attenuate auxin signals. Nature **419,** 167–170.

Yin, Y., Wang, A.-Y., Mora-Garcia, S., Li, J., Yoshida, S., Asami, T., and Chory, J. (2002). BES1 accumulates in the nucleus in response to brassinosteroids to regulate gene expression and promote stem elongation. Cell **109,** 181–191.

Zaina, S., Brevaiaro, D., Mappelli, S., Bertani, A., and Reggiani, R. (1994). Two putative G protein a subunits dissociate from rice coleoptile membranes after GTP stimulation. J. Plant Physiol. **143,** 293–297.

Zaina, S., Mappelli, S., Reggiani, R., and Bretani, A. (1991). Auxin and GTPase activity in membranes from aerobic and anaerobic rice coleoptiles. J. Plant Physiol. **138,** 760–762.

Zaina, S., Reggiani, R., and Bertani, A. (1990). Preliminary evidence for involvement of GTP-binding protein(s) in auxin signal transduction in rice (*Oryza sativa* L.) coleoptile. J. Plant Physiol. **136,** 653–658.